PCCP

Accepted Manuscript

ROYAL SOCIETY OF CHEMISTRY

www.rsc.org/pccp

Insights into the effects of mutations on Cren7-DNA binding using molecular dynamics simulation and free energy calculation

Lin Chen,[ab] Qing-Chuan Zheng*[a] and Hong-Xing Zhang[a]

[a] *International Joint Research Laboratory of Nano-Micro Architecture Chemistry, State Key Laboratory of Theoretical and Computational Chemistry, Institute of Theoretical Chemistry, Jilin University, Changchun 130023, P. R. China.*

[b] *College of Chemistry and Chemical Engineering, Qiqihar University, Qiqihar 161006, P. R. China*

E-mail: zhengqc@jlu.edu.cn; Tel: +86-431-88498966; Fax: +86-431-88498966

Abstract

A novel, highly conserved chromatin protein, Cren7 is involved in regulating essential cellular processes such as transcription, replication and repair. Although mutations in the DNA-binding loop of Cren7 destabilize the structure and reduce DNA-binding activity, the details are not very clear. Focused on the specific Cren7-dsDNA complex (PDB code 3LWI), we applied molecular dynamics (MD) simulations and the molecular mechanics Poisson-Boltzmann surface area (MM-PBSA) free energy calculation to explore the structural and dynamic effects of W26A, L28A, and K53A mutations in comparison to the wild-type protein. The energetic analysis indicated that the intermolecular van der Waals interaction and nonpolar solvation energy play an important role in the binding process of Cren7 and dsDNA. Compared with the wild type Cren7, all the studied mutants W26A, L28A, and K53A have obvious reduced binding free energies with dsDNA in the reduction of the polar and/or nonpolar interactions. These results further elucidated the previous experiments to understand the Cren7- DNA interaction comprehensively. Our work also would provide

support to understand the interactions of proteins with nucleic acids.

Introduction

Protein-DNA interactions in biological systems are the foundation of many important cellular processes, such as growth, cell division, differentiation, and gene expression.[1,2] Comprehension of the interactions and binding mechanism between protein and DNA is fundamental to elucidate protein function and is the most puzzling issue of modern structural biology.[3,4] Although X-ray crystallography, nuclear magnetic resonance (NMR), and neutron diffraction studies can provide some significant information for the interactions of proteins and DNA, they are not given a dynamic description. In recent years, many scientists have used the molecular dynamics (MD) simulation procedures[5-14] to investigate the molecular basis of protein-DNA interactions at atomic level and at the appropriate time scale.

The chromatin protein Cren7 was first highly conserved protein detected in Crenarchaetoa that plays a key role in the DNA packaging. Cren7 is also involved in regulating essential cellular processes such as transcription, replication and repair. The 6.6 kDa Cren7 protein is a small nonspecific DNA-binding protein, stabilizing dsDNA and constraining negative DNA supercoils. MD studies[15] have also investigated the role of Cren7 in facilitating the stabilization and structural transitions of DNA depending on temperature. Based on X-ray crystallography studies[16,17] on several structures of Cren7, it adopts an SH3-like fold with 60 amino acid residues. The Cren7-DNA complex structure, illustrated in Figure 1, shows that the protein interacts with duplex DNA through a triple-stranded β-sheet (β3、β4、β5) and a long flexible loop (loop β3-β4). Previous experimental studies[17] have shown that loop β3-β4 plays a fundamental role in the binding of the protein to DNA.

Although the reported crystal structure of Cren7-dsDNA complex can provide plentiful atomic-level structural information for understanding the structural basis of the interactions of dsDNA and Cren7, the molecular details of Cren7-dsDNA interactions are still unclear. Additionally, the experiments indicate the mutations of residues on the dsDNA-binding surface, such as W26, L28, and K53, which are directly related to dsDNA-binding, will highly reduce binding affinity with the dsDNA. The details of these mutants reducing dsDNA binding are not clear. We also need to understand the origin of affecting the binding affinity of Cren7 and dsDNA. These problems can be used MD simulations combined with binding free energy calculations investigate at atomic level. These methods can provide plentiful structure-dynamical information for protein-DNA in solution, and also provide a wealth of energetic information. Such information is of great importance to understand the essence of protein-DNA interactions, whereas they cannot be provided by experimental studies.

In our work, to understand why the mutations of residues such as W26, L28, and K53 resulting in the loss of dsDNA binding affinity by Cren7 protein, as well as to characterize the key residues in the interaction between Cren7 protein and dsDNA, MD simulations and molecular mechanics/Poisson-Boltzmann surface area (MM-PBSA) approach were performed on the wild type and mutated Cren7 protein with dsDNA complexes. These simulations can complement experiments for better understanding of the interactions between Cren7 protein and dsDNA by providing atomic details that are often inaccessible in experiment due to resolution and the MM-PBSA calculation will help us understand which features will determine the Cren7-dsDNA binding process.

Materials and methods

Initial models of systems

The initial crystal structure of Cren7-dsDNA complex in this study was obtained from the Protein Data Bank (PDB code: 3LWI) [17]. Based on the wild type structure, we generated the starting structure of mutants W26A, L28A, and K53A by substituting the corresponding residues using Discovery Studio 2.5 software package[18] and the mutated residues were shown in Figure 1.

Molecular dynamics simulations

All other calculations and MD simulations were carried out with AMBER 11 software package[19] using the classical ff03 force filed[20]. Sodium ions (Na^+) were added using the *xLEAP* module to neutralize the system based on a coulomb potential grip. Each system was then solvated with the TIP3P water model[21] in a truncated octahedron boxes. The minimum distance from any solute atom to the edge of the box was 10 Å. The solvated systems were energy minimized for 1500 steps of steepest descent (SD) method followed by a further 3000 steps of conjugated gradient algorithms for each system, with 100 kcal mol^{-1} $Å^{-2}$ restraints on the protein/DNA. Subsequently, these initial harmonic restraints were gradually reduced to zero during a series of progressive energy minimizations. After that the systems were gently heated from 50 to 300 K applying harmonic restraints with a force constant of 5 kcal mol^{-1} $Å^{-2}$ on the solute atoms, and then equilibrated for 500 ps. Finally, production MD simulations were then carried out for 30 ns under an *NPT* ensemble. During the minimizations and MD simulations, Particle Mesh Ewald (PME) [22] was used to treat the long-range electrostatic interactions with a periodic boundary condition. All bonds involving hydrogen atoms were restricted by the SHAKE algorithm[23]. The times step of 2 fs was used in all MD simulations.

The PyMOL[24] and VMD software[25] were used to visualize the trajectories and to depict structural representations.

Binding free energy calculation

Binding free energy calculations were carried out based on MM-PBSA method[26-28] using the extracted snapshots from the last 5 ns trajectories. In this method, the binding free energies (ΔG_{bind}) are computed as in eq.(1):

$$\Delta G_{bind} = G_{complex} - G_{protein} - G_{DNA} \quad (1)$$

$G_{complex}$, $G_{protein}$, and G_{DNA} are the free energies of complex, protein and DNA, respectively. The free energy ($G_{x = complex, protein, DNA}$) can be computed by the following scheme using the MM-PBSA methods:

$$G_{x = complex, protein, DNA} = E_{MM} + G_{solv} - TS \quad (2)$$

$$E_{MM} = E_{ele} + E_{vdw} + E_{int} \quad (3)$$

$$G_{solv} = G_{pb} + G_{nonp} \quad (4)$$

E_{MM} is the gas phase energy, G_{solv} is the solvation free energy, E_{ele}, E_{vdw}, and E_{int} are the electrostatic energy, the van der Waals interaction energy and the internal energy, respectively. The solvation free energy, G_{solv}, can be decomposed into electrostatic solvation energy (G_{pb}) and non-electrostatic solvation energy ($G_{nonpolar}$). The polar component (the electrostatic solvation energy) is computed using the Poisson-Boltzmann (PB)[29,30]. The dielectric constants for the solute and the surrounding solvent were set to 1 and 80[31,32] respectively, and the ionic strength was set to 0.1 M. The non-polar contribution (the non-electrostatic solvation energy) is estimated to use the scheme as follows:

$$G_{nonpolar} = \gamma * SASA + \beta \quad (5)$$

The γ and β, two empirical constants, were set as 0.00542 kcal mol^{-1} $Å^{-2}$ and 0.92 kcal mol^{-1},[33,34] SASA is the solvent accessible surface area determined by a probe radius of 1.4 Å. The solute entropy S[35] is estimated by normal mode analysis using the normal module analysis[36]. We took 100 snapshots from the last 5 ns trajectory at an interval of 50 ps to calculate the entropy contribution.

To obtain a detailed view of Cren7-dsDNA binding, the MM-GBSA energy decomposition was performed to address the contributions of each residue to the binding free energies, which can provide a full description of energetic influences on binding affinity. For the decompositions of MM-GBSA free energy calculations, the solvation energies were not consideration the contribution of entropies.

Results and discussion

Stability of Cren7-DNA complexes

To check the stability of the MD simulations, the root-mean square deviation (RMSD) of the backbone atoms of Cren7-dsDNA complexes are plotted (Figure 2). As Figure 2 shows, after the initial 5 ns MD simulations, most of the systems are up to equilibration except L28A mutant. L28A mutant becomes to be stabilized only after 25 ns. To compare the structural differences, we analyzed the time evolution of RMSD of backbone atoms averaged for each residue in Cren7 protein. The average RMSD of backbone atoms for wild type, W26A, L28A, and K53A are 1.56，1.66，1.99 and 1.60 Å, respectively, indicating that the equilibrated structures are very similar to the crystal structure and the involved mutations do not change the backbone structure largely.

To further evaluate the convergence of the MD simulations, the time evolution of the

enthalpy and entropy was calculated based on the last 5 ns trajectories for each simulation (Figures 3 and 4). Since the conformation change occurs for Cren7 and DNA upon the formation of the complex, the enthalpies and entropies are quite variable, but the accumulated mean values became stable quickly after a short length of MD simulation. In a word, all the four systems are stable during the last 5 ns MD simulations.

Calculation of binding free energy of wild type system

To investigate the source of governing binding and the loss of binding affinity in mutants, the detailed contributions of various energy components computed by MM-PBSA and the entropy contributions from the normal-mode analysis are given (Table 1). As can be seen from Table 1 and Figure 4, the change of entropy during the formation of Cren7-dsDNA complex is large, indicating the large conformation change occurs for Cren7 and DNA upon the formation of complex. Of individual energy contribution, the major favorable contributions to the binding process comes from the nonpolar solvation energy ($\Delta G_{nonpolar} = E_{vdw} + G_{np}$) with -107.02 kcal/mol, more specifically from the van der Waals energy (E_{vdw}). Van der Waals energy is eleven times stronger than non-electrostatic solvation energy (ΔG_{np}). Relative to the nonpolar solvation energy ($\Delta G_{nonpolar}$), the polar solvation energies (ΔG_{polar}) make unfavorable contribution to the binding energy. In general, the nonpolar interactions energy are highly favorable to the binding process but their contributions are compensated by the polar solvation interactions energies penalties associated with the binding between the Cren7 and DNA.

To identify and characterize the hotspot residues of the Cren7-DNA interaction interface, per-residue free energy decomposition was employed and the corresponding results were

given (Figures 5 and 6). From Figure 5, we can see that there are 12 residues (Lys24、Trp26、Leu28、Pro30、Lys31、Arg33、Val36、Ile38、Leu40、Tyr49、Arg51、and Lys53) for Cren7 have more than 2 kcal/mol free energy contribution to its binding to DNA. Figure 6 also gives a graphically display for the distribution of the 12 important residues. In general, the identified hotspot residues lie in the binding surface and they can form the direct interaction with DNA. These direct interactions form the recognition basis of Cren7 protein and DNA. Among these residues, five amino acid residues (Lys24、Trp26、Leu28、Arg51、and Lys53) make major contributions to the binding free energy with more than 5 kcal/mol. For DNA, two regions have important contributions for binding between the Cren7 and DNA. one region consists of bases A3、A4、T13、T14 and A15, the other region includes two bases T5 and T6. These identified residues based on binding free energy calculations are very important for the Cren7-DNA binding. Most of them have been proved to be crucial for the Cren7-DNA binding from experiments[16]. For instance, the residues participating in the interaction with dsDNA include the hydrophobic/aromatic residues (Trp26、Leu28、Pro30、Val36、Ile38、Leu40) and the positively charges residues (Lys24、Lys31、Arg33、Arg51、and Lys53). In addition, The residues Lys24 and Leu28 form hydrophobic interactions with the bases of A3、A4、T5、T6、T13、T14 and A15. In our calculation, Leu28 residue have 7.65 kcal/mol binding energy binding contribution. From surface Plasmon resonance assays, L28A mutations decrease the dsDNA-binding affinity by 54-fold.

To investigate thoroughly the origin of the large contribution from the key residues, we further decompose binding free energy into variable contributions on these residues. The binding free energy can be divided into polar and nonpolar interaction generally. By

analyzing the contribution of individual energy during the process of Cren7-DNA complex formation, the nonpolar interaction energy ($\Delta G_{nonpolar}=E_{vdw} + G_{np}$) has -107.02 kcal/mol contribution and the polar interaction energy ($\Delta G_{polar}= E_{ele} + G_{pb}$) has 19.10 kcal/mol contribution. While, we pay close attention to which residues should be responsible for each energy terms. To answer this question, the contribution of the identified 12 key residues is further decomposed into polar and nonpolar section in Figure 7. It can be seen that most of important resides for Cren7 have a large nonpolar interaction contribution. For example, two important residues Trp26 and Leu28, whose mutation into alanine will decrease the dsDNA-binding affinity by 30- and 54-fold, display their contribution to binding process only from the nonpolar interaction. While the other three residues K24, R33 and K53 have obvious polar and nonpolar contribution for the binding between the Cren7 and DNA. For example, K53A mutations decrease the dsDNA-binding affinity by 24-fold, display their contribution to binding process from both the nonpolar interaction and polar interaction.

Binding affinity loss for mutants

To investigate the source of binding affinity loss for the studied mutants, we calculated the binding free energy and the individual energy contribution to the binding of Cren7 with DNA based on the last 5 ns MD simulations (Table 1). It is well known that formation of Cren7-DNA complex is opposed by a loss in configurational entropy of the binding partners. By analyzing the interface residues of Cren7-DNA complex, these three hydrophobic residues (W26, L28) are buried into the interior of the complex upon binding, which should contribute to the solvent entropy change. At the same time, the mutation of K53 to alanine makes the Cren7-DNA interaction disappear largely, which should contribute to the loss of solute

conformational degrees of freedom. As shown in the Table 1 and Figure 4, the corresponding entropy contributions for the three mutant systems are different from the wild system, with the values ranging from 31.64 to 34.82 kcal/mol, This is because the entropic contributions results from the conformational changes in rotational, translational and vibrational degrees of freedom of solute upon complex formation. In general, the studied mutated systems have a smaller binding free energy relative to wild type. The binding free energy of wild type, W26A, L28A, and K53A are -52.19，-37.57，-31.20，and -38.48 kcal/mol respectively. Based on the order of binding free energies, the DNA binding potencies with the WT and mutated Cren7 protein can be ranked as: WT> K53A> W26A > L28A. This rank is well consistent with the experimental result[17]. As reported in the reference, the mutants W26A and K53A decrease the dsDNA binding affinity by 30- and 24-fold. However, L28A mutant decrease the dsDNA binding affinity by 54-fold.

Through the comparison the individual energy contribution for wild type and different mutants, we could ascertain the source of binding affinity loss for the studied mutants. As seen from Table1, both the polar and nonpolar contributions of binding energies reduced largely for L28A, and K53A mutants relative to the wild type system. For example, the polar interaction contribution decreased 13.12 kcal/mol and 12.36 kcal/mol as well as the nonpolar contribution decreased 8.79 kcal/mol and 5.44 kcal/mol, respectively for L28A, and K53A mutants compared with the wild type system. As for the W26A mutant, only the nonpolar contribution reduces with 15.95 kcal/mol, the polar contribution shows a slight decline. These results are well consistent with the experimental results[17]. As reported in the reference, the mutants W26A and K53A decrease the dsDNA binding affinity only from the nonpolar

interactions, K53A mutations decrease the dsDNA-binding affinity from both the nonpolar interaction and polar interaction.

For the purpose of investigation which residues are accountable for the reduced binding free energy for the studied mutants, we further decompose the binding free energy into the contribution from each residue and plot the contribution difference of per residue for the mutated and wild type Cren7 protein (Figure 8). As for the W26A and K53A mutants, basically, only W26A and K53A mutated residues are responsible for the binding affinity decreasing. For example, the mutation from W26 to A26 makes the free energy contribution of the residue 26 decrease obviously form -5.89 kcal/mol to -1.14 kcal/mol, and the mutation from K53 to A53 makes the free energy contribution of the residue 53 decrease obviously from -5.58 kcal/mol to -0.95 kcal/mol. By analyzing the change of DNA residues' contributions, we can make out that the binding affinity decreasing of W26A and K53A should contribute to the disappearing of the interaction between residue 26 from Cren7 and T5 from DNA, and the binding affinity decreasing of K53A should contribute to the disappearing of the interaction between residue 53 from Cren7 and A15 from DNA. As for the L28A mutants, not only the mutated residues but also other residues such as Lys31and Arg51 exert the obvious reduced contribution for Cren7 protein binding to DNA, indicating that the L28A mutant entirely interrupt the formation of Cren7 protein with DNA.

To search the origin of the loss of the above residues' contribution, we further analyze the difference of per-residue polar and nonpolar contributions between the mutated and wild type system and give the corresponding results in Figure 9. For W26A mutant, the loss of nonpolar contribution of residue 26 is the main reason of the binding affinity decreasing. On the

contrary, for K53A mutant, the loss of polar contribution of residue 53 is the main reason of the binding affinity decreasing. As for the L28A mutant, not only the loss of nonpolar contribution of residue 28 but also the loss of polar contribution of other residues is the main reason of the binding affinity decreasing. In order to explore the structural detail changes between mutant and wild type system, clustering analysis was applied to extract the conformation that best represents the whole ensemble. During the clustering analysis, the self-organization map method form the AMBER ptraj module was used to cluster the MD trajectories based on the pairwise similarity measured by RMSD of the backbone atoms. The largest cluster was chosen and shown in Figure 10. We can see clearly that the mutation from a large and polar residue W26 to a small and neural residue alanine makes the important interactions which take a primary role to anchor DNA and keeps DNA binding to Cren7 protein well, resulting in a large decreasing of DNA binding affinity to Cren7. For L28A mutant, it can be seen that the DNA structure distorts on some degree, resulting in a large decreasing of DNA binding affinity to Cren7. For K53A mutant, the positively charged residues K53 have made important contributions to DNA binding through the formation of hydrogen bonds and salt bridges. The mutation of K53 to alanine makes such strong electrostatic interaction disappear largely.

Conclusions

In this study, MD simulations and binding free energy calculation were performed to investigate why these mutations result in the loss of dsDNA binding affinity by Cren7 protein. The results of binding free energy decomposition indicated that the nonpolar solvation interactions dominate the binding of Cren7 and DNA. By comparing the individual energy

contributions of the mutated and wild type system, the source of binding affinity decreasing for different mutants is different. For L28A and K53A mutants, both the polar and nonpolar contributions of binding energies reduced largely compared with the wild type system. For the W26A mutant, only the nonpolar contribution reduced largely compared with the wild type. Through the decomposition the binding free energy into the contribution from each residue, 12 conserved amino acid residues (Lys24、Trp26、Leu28、Pro30、Lys31、Arg33、Val36、Ile38、Leu40、Tyr49、Arg51、and Lys53) make major contributions for Cren7-DNA binding. All the key residues by experimental identification are included in our identified residues group. The detailed understanding of Cren7-dsDNA interaction will provide some useful insights and new chances for the Cren7 protein.

Acknowledgements

This work is supported by Natural Science Foundation of China (Grant Nos. 21273095).

References

1 J. Iwahara, C. D. Schwieters and G. M. Clore, *J. Am. Chem. Soc.*, 2004, **126**, 12800-12808.

2 C. G. Kalo imos, N. Biris, A. M. J. J. Bonvin, M. M. Levandoski, M. Guennuegues, R. Boelens and R. Kaptein, *Science*, 2004, **305**, 386-389.

3 G. MacBeath, *Nat. Genet.*, 2002, **32**, 526-532.

4 G. D. Stormo and D. S. Fields, *Trends Biochem. Sci.*, 1998, **23**, 109-113.

5 M. J. Shoura, R. J. K. Ranatunga and S. A. Harris, *Biophys. J.*, 2014, **107**, 700-710.

6 B. R. Miller III, C. A. Parish and E. Y. Wu, *PLoS Comput. Biol.*, 2014, **10**, e1003961.

7 M. J. Shoura, R. U. Ranatunga, S. A. Harris, S. O. Nielsen and S. D. Levene, *Biophys. J.*, 2014, **107**, 700-710.

8 M. Li, B. A. Shoemaker and R. R. Thangudu, *J. Phys. Chem. B*., 2013, **117**, 13226-13234.

9 I. Dannessa, A. Coletta and T. Sutthibutpong, *Nucleic. Acids. Res.*, 2014, **42**, 9304-9312.

10 I. D'Annessa, A. Coletta, T. Sutthibutpong, J. Mitchell, G. Chillemi, S. Harris, and A. Desideri, *Nucleic. Acids. Res.*, 2014, **42**, 9304-9312.

11 R. Tapia-Rojo, J. J. Mazo, J. Á. Hernández, M. L. Peleato, M. F. Fillat and F. Falo, *PLoS Comput. Biol.*, 2014, **10**, e1003835.

12 N. Santa Singh, S. Kachhap, R. Singh, R. C. Mishra, B. Singh and S. Raychaudhuri, *Mol. Genet. Genomics*, 2014, **289**, 1171-1182.

13 A. Bhattacherjee and Y. Levy, *Nucleic. Acids. Res.*, 2014, **42**, 12404-12414.

14 N. M. Walavalkar, J. M. Cramer, W. A. Buchwald, J. N. Scarsdale and D. C. Williams, *Nucleic. Acids. Res.*, 2014, **42**, 11218-11232.

15 L. Chen, J. Zhang, L. Yu, Q. Zheng, W. Chu, Q. Xu, H. Zhang and C. Sun, *J. Phys. Chem. B*., 2012, **116**, 12415-12425.

16 L. Guo, Y. Feng, Z. Zhang, H. Yao, Y. Luo, J. Wang and L. Huang, *Nucleic. Acids. Res.*, 2008, **36**, 1129-1137.

17 Z. Zhang, Y. Gong, L. Guo, T. Jiang and L. Huang, *Mol. Microbiol.*, 2010, **76**, 749-759.

18 D. Studio, Version 2.5, Accelrys Inc.: San Diego, CA, 2009.

19 D. Case, T. Darden, T. Cheatham, C. Simmerling, J. Wang, R. Duke, R. Luo, R. Walker, W. Zhang and K. Merz, *AMBER 11*, University of California, San Francisco, 2010.

20 Y. Duan, C. Wu, S. Chowdhury, M. C. Lee, G. Xiong, W. Zhang, R. Yang, P. Cieplak, R. Luo and T. Lee, *J. Comput. Chem.*, 2003, **24**, 1999-2012.

21 W. L. Jorgensen, J. Chandrasekhar, J. D. Madura, R. W. Impey and M. L. Klein, *J. Chem. Phys.*, 1983, **79**, 926-935.

22 T. Darden, D. York and L. Pedersen, *J. Chem. Phys.*, 1993, **98**, 10089-10092.

23 J. P. Ryckaert, G. Ciccotti and H. J. C. Berendsen, *J. Comput. Phys.*, 1977, **23**, 327-341.

24 W. L. DeLano, *The PyMol molecular graphics system*, DeLano Scientific, San Carlos, CA, 2002.

25 W. Humphrey, A. Dalke and K. Schulten, *J. Mol.Graph.*, 1996, **14**, 33-38.

26 J. Srinivasan, T. E. Cheatham, P. Cieplak, P. A. Kollman and A. David, *J. Am. Chem. Soc.*, 1998, **120**, 9401-9409.

27 J. M. J. Swanson, R. H. Henchman and J. A. McCammon, *Biophys. J.*, 2004, **86,** 67-74.

28 T. Hou, J. Wang, Y. Li and W. Wang, *J. Chem. Inf. Model.*, 2011, **51**, 69-82.

29 D. Bashford and D. A. Case, *Annu. Rev. Phys. Chem.*, 2000, **51**, 129-152.

30 R. Luo, L. David and M. K. Gilson, *J. Comput. Chem.*, 2002, **23**, 1244-1253.

31 B. Yang, Y. Zhu, Y. Wang and G. Chen, *J. Comput. Chem.*, 2011, **32**, 416-428.

32 S. Milev, A. A. Gorfe, A. Karshikoff, R. T. Clubb, H. R. Bosshard and I. Jelesarov, *Biochemistry-us*, 2003, **42**, 3481-3491.

33 D. Sitkoff, K. A. Sharp and B. Honig, *J. Phys. Chem.*, 1994, **98**, 1978-1988.

34 T. E. Cheatham, J. Srinivasan, D. A. Case and P. A. Kollman, *J. Biomol. Struct. Dyn.*, 1998, **16**, 265-280.

35 H. Gouda, I. D. Kuntz, D. A. Case and P. A. Kollman, *Biopolymers*, 2003, **68**, 16-34.

36 D. A. Case, *Curr. Opin. Struc. Biol.*, 1994, **4**, 285-290.

Table

Table 1. Calculated binding free energy and its components (kcal/mol) of the wild type and mutated Cren7-dsDNA complexes.

	WT	W26A	L28A	K53A
E_{ele}	-2540.70	-2307.51	-2120.03	-1960.79
E_{vdw}	-98.56	-82.87	-90.56	-93.85
ΔE_{MM}	-2639.26	-2390.38	-2210.60	-2054.73
G_{np}	-8.46	-8.20	-7.67	-8.00
G_{pb}	2559.80	2326.74	2152.25	1992.25
ΔG_{solv}	2551.34	2318.54	2144.58	1984.25
ΔG_{polar}	19.10	19.23	32.22	31.46
$\Delta G_{nonpolar}$	-107.02	-91.07	-98.23	-101.58
ΔH_{bind}	-87.92	-71.84	-66.02	-70.12
$T\Delta S$	-35.73	-34.27	-34.82	-31.64
ΔG_{bind}	-52.19	-37.57	-31.20	-38.48

$\Delta G_{polar} = E_{ele} + G_{pb}$

$\Delta G_{nonpolar} = E_{vdw} + G_{np}$

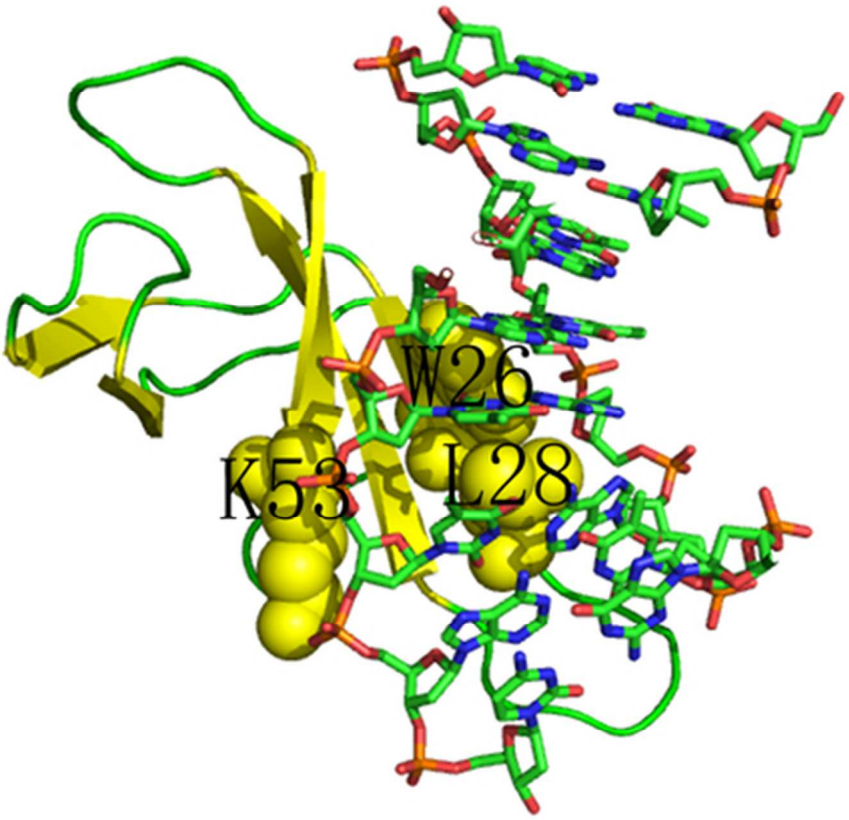

Fig1 : The Cren7-DNA complex (PDB ID: 3LWI). Cren7 is given in the cartoon representation, and the mutated residues W26, L28, and K53 are given in the sphere representation.
39x35mm (300 x 300 DPI)

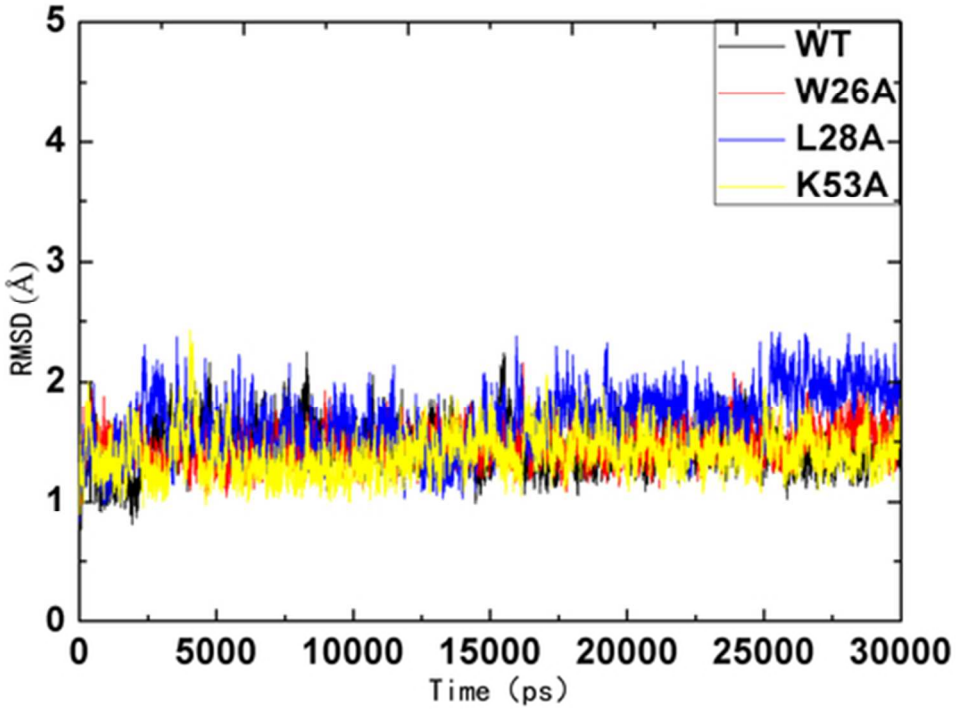

Fig2:Time dependence of the RMSD values of protein investigated in the present paper from the initial structures extracted from the Cren7-DNA complex. The black lines show RMSDs of the wild type protein. The red lines represent RMSDs of the W26A mutant. The blue lines correspond to RMSDs of the L28A mutant. The yellow lines show RMSDs of the K53A mutant.
40x30mm (300 x 300 DPI)

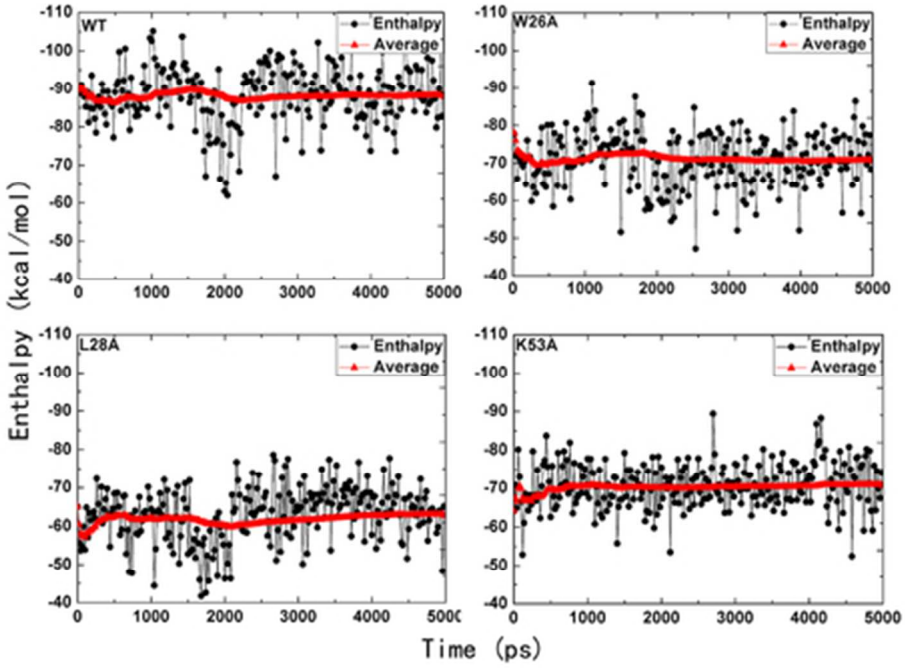

Fig3:The fluctuations and accumulated mean values of enthalpies for the Cren7-DNA, W26A-DNA, L28A-DNA, K53A-DNA complexes
40x28mm (300 x 300 DPI)

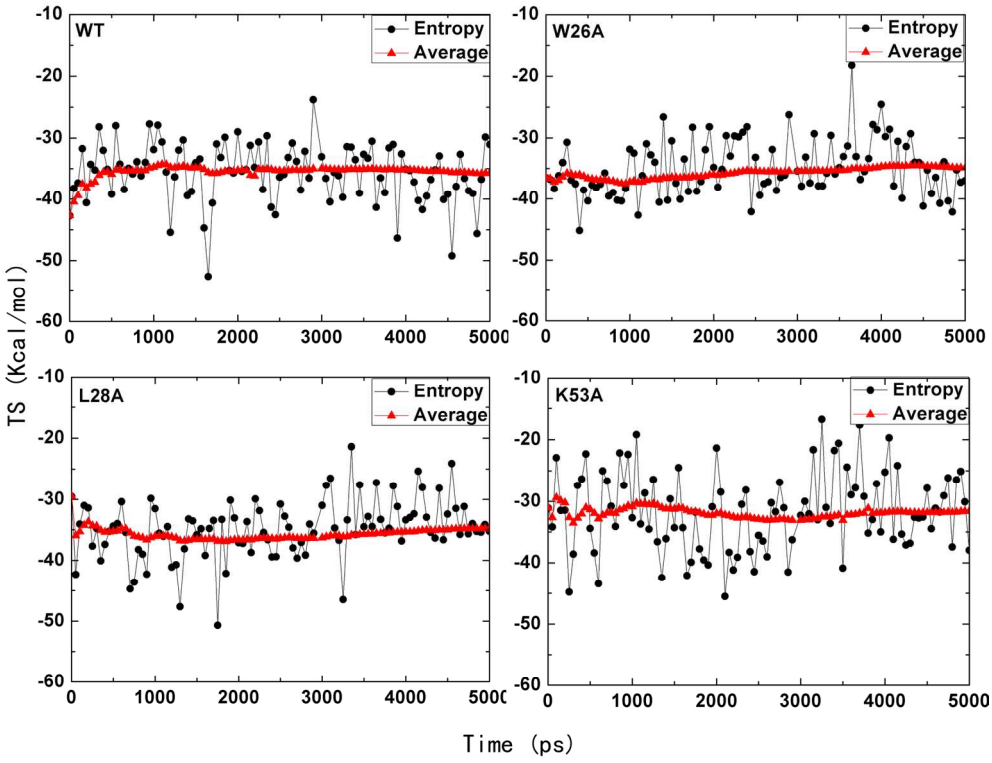

Fig4:The fluctuations and accumulated mean values of entropies for the Cren7-DNA, W26A-DNA, L28A-DNA, K53A-DNA complexes.
157x122mm (300 x 300 DPI)

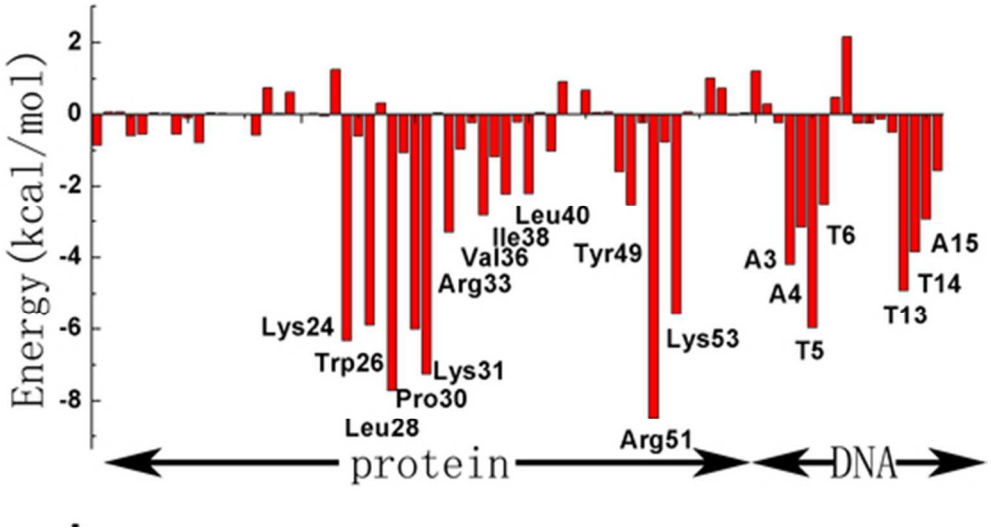

Fig5:The corresponding energy contributions of hotspot residues of Cren7 (kcal/mol)
45x24mm (300 x 300 DPI)

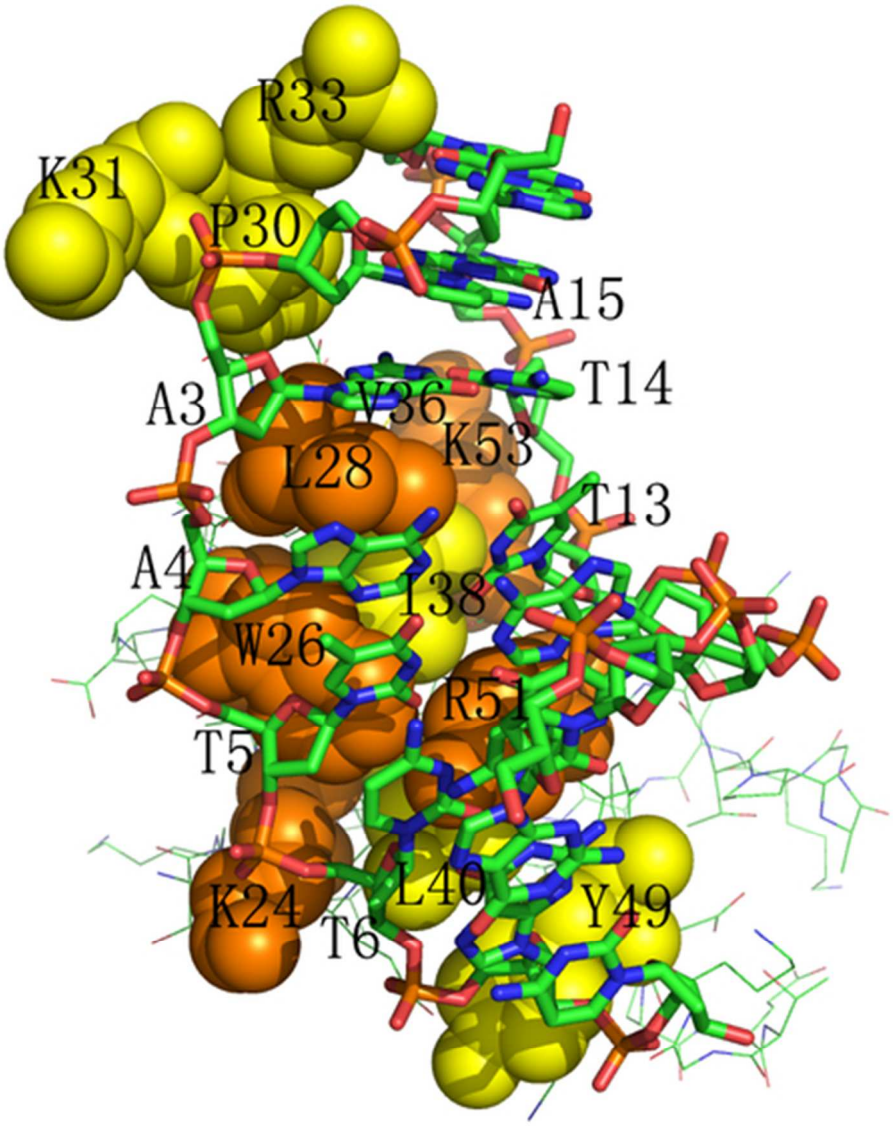

Fig6 : The hotspot residues of Cren7 for the interaction of Cren7 and dsDNA
39x49mm (300 x 300 DPI)

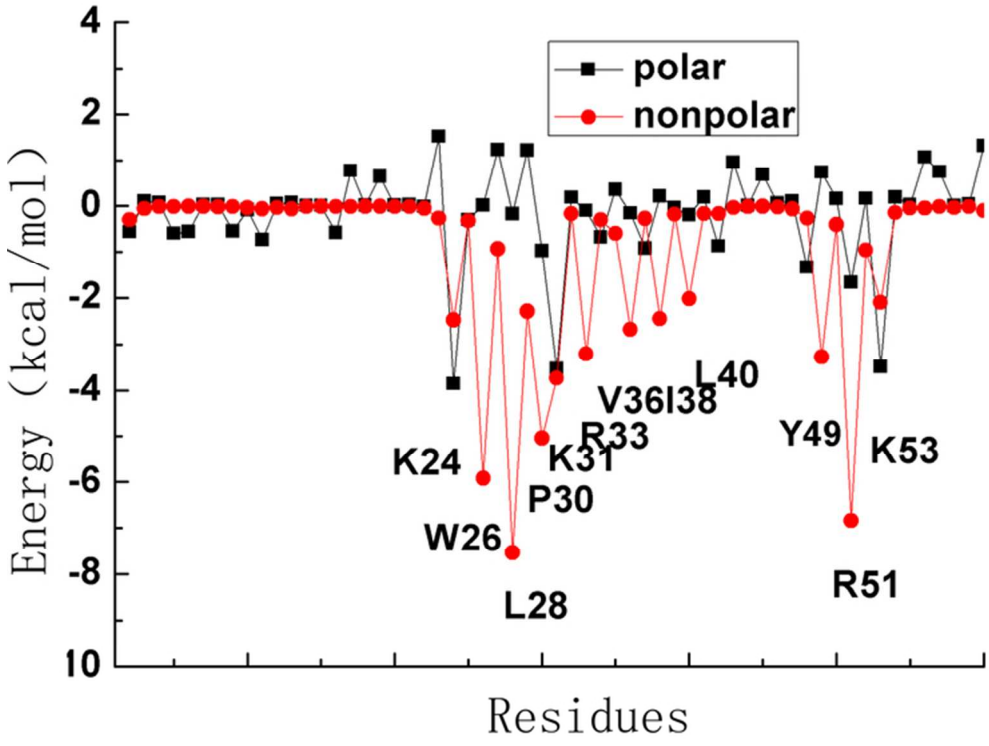

Fig7 : The polar and nonpolar interaction contributions for the identified key residues of Cren7.
63x48mm (300 x 300 DPI)

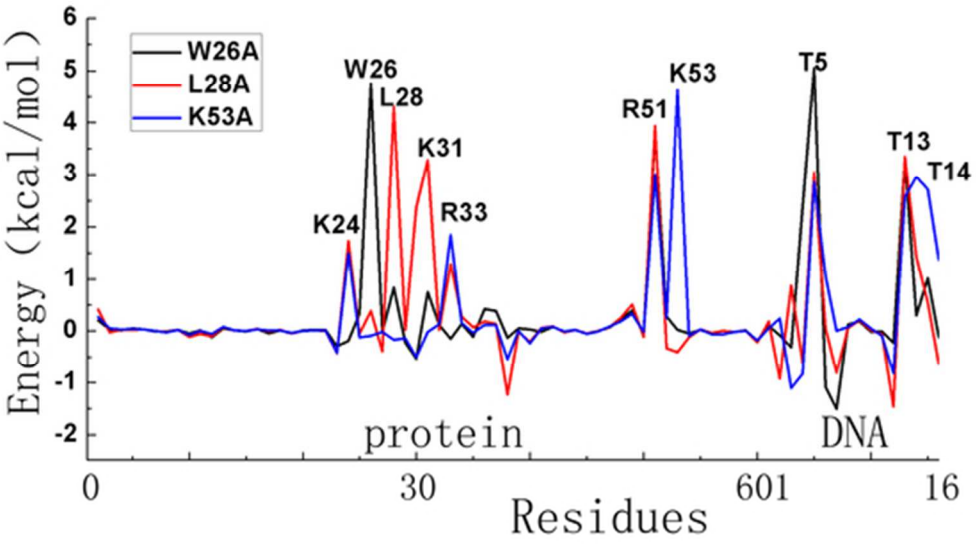

Fig8:Energy contribution difference of each residue for the mutated Cren7-DNA binding relative to the wild type Cren7-DNA binding
47x26mm (300 x 300 DPI)

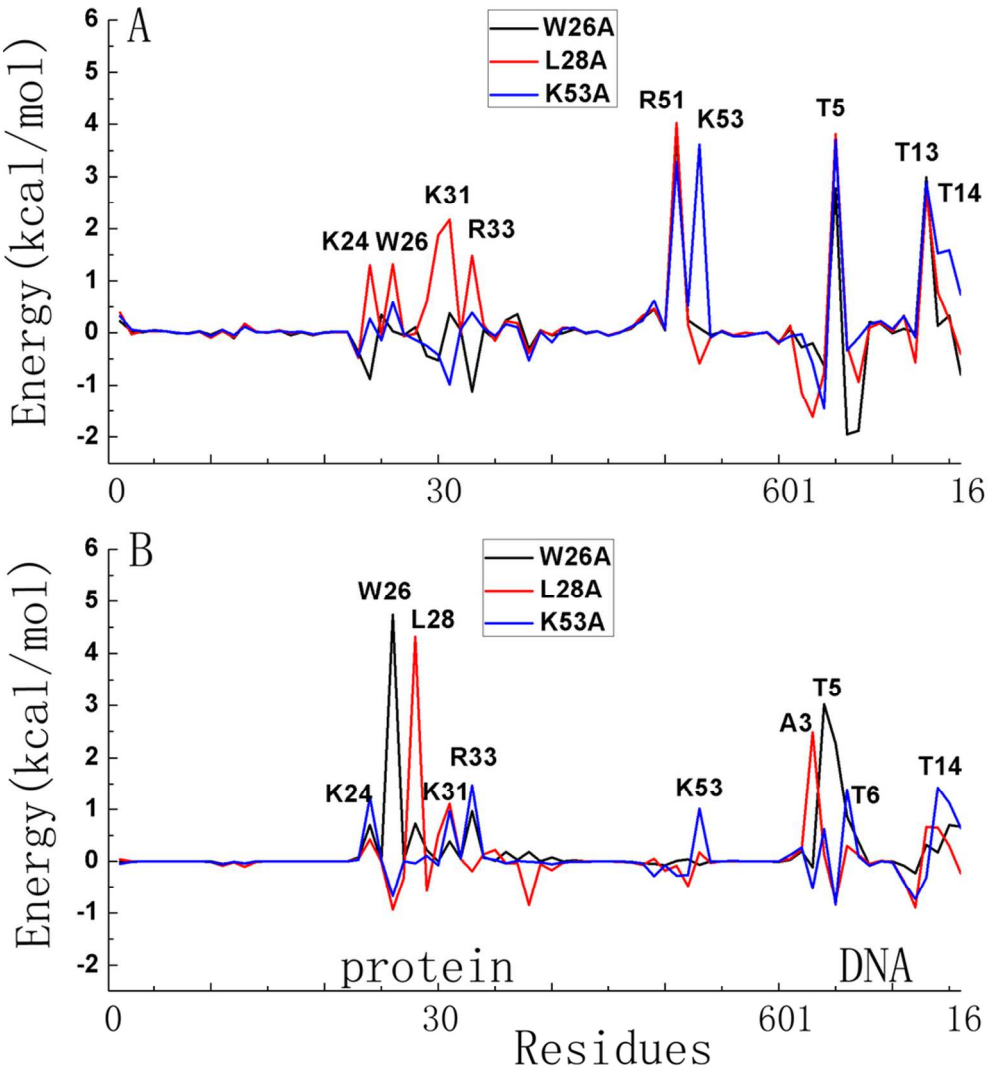

Fig9 : Energy contribution difference of each residue for the mutated Cren7-DNA binding relative to the wild type Cren7-DNA binding: (A) the polar contribution; (B) the nonpolar contribution.
91x98mm (300 x 300 DPI)

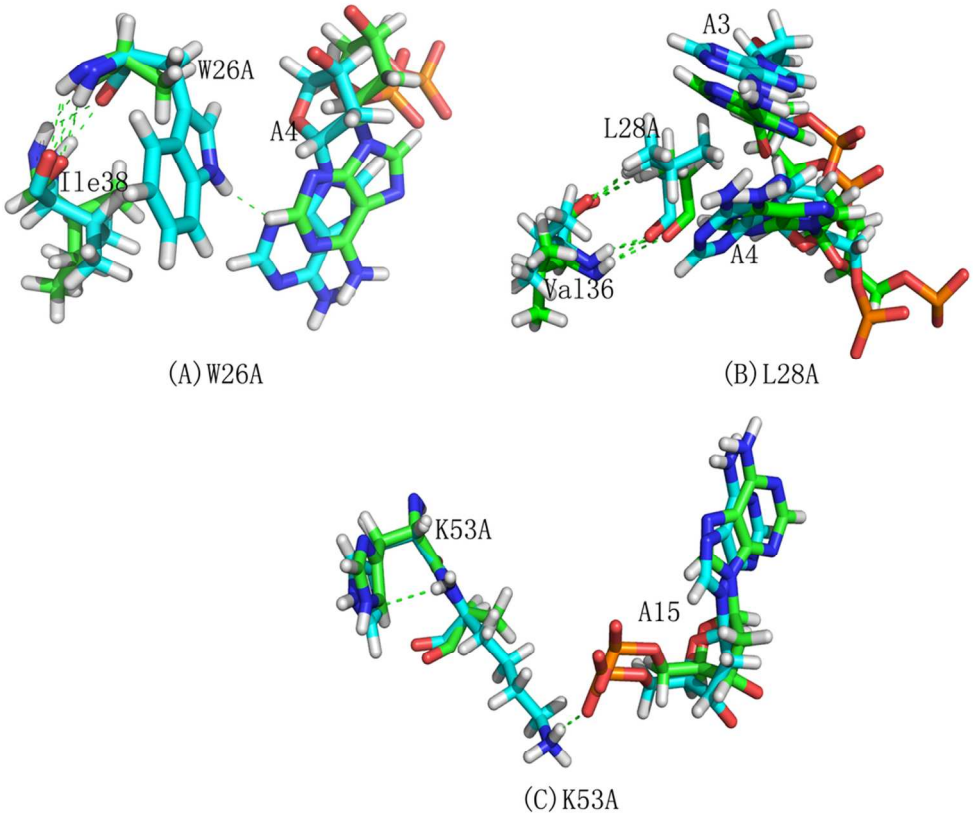

Fig10:The comparison of key interactions between the wild type and studied mutants (carbon atoms of all the mutants are colored by blue, carbon atoms of all the mutants are colored by green)
98x86mm (300 x 300 DPI)